Pramāṇa, Vol. 24, Nos 1 & 2, January & February 1985, pp. 293–310. © Printed in India.

Electron energy loss spectroscopy (EELS) of organic molecules in vapour phase: Design and fabrication of an indigenous EEL spectrometer*

M S HEGDE, V JAYARAM, P VISHNU KAMATH and C N R RAO†

Solid State and Structural Chemistry Unit, Indian Institute of Science, Bangalore 560 012, India

Abstract. An indigenous electron energy loss spectrometer has been designed and fabricated for the study of free molecules. The spectrometer enables the recording of low-resolution electronic spectra of molecules in the vapour phase with ready access to the vacuum ultraviolet region. Electron energy loss spectra of aliphatic alcohols and carbonyl compounds as well as of benzene derivatives have been recorded with the indigenous spectrometer and the electronic transitions in these molecules discussed.

Keywords. Electron energy loss spectroscopy; vacuum ultraviolet spectroscopy; EELS.

PACS No. 33·20; 34·80

1. Introduction

Electron energy loss spectroscopy (EELS) provides an effective means of investigating electron states of free atoms and molecules (Celotta and Huebner 1979; Rao *et al* 1980). In this technique, a primary electron beam of energy E_i, collides with atoms or molecules and the inelastic collisions cause excitations within the sample. The kinetic energy E_f of the inelastically scattered electrons is measured and the difference, $\Delta E = E_i - E_f$, directly gives the energy absorbed by the molecule during the collision process (figure 1). EELS is similar to optical absorption spectroscopy, but the advantage of EELS lies in the fact that it can be utilised to study optically forbidden transitions (Kuppermann *et al* 1979; Koerting *et al* 1984). The phenomenon of electron exchange (Oppenheimer 1928) whereby the scattered electron is different from the incident one, enables us to study spin-forbidden transitions. Symmetry-forbidden transitions in molecules can also be observed since the incident electron can polarize the electron cloud distribution of the molecule during collision.

What is specially significant about EELS is that it gives us ready access to the vacuum UV region of electronic spectroscopy and this in conjunction with photoelectron spectroscopy provides the complete molecular energy level diagram of the molecule under study. Since an EELS instrument is relatively simple and inexpensive to fabricate, it can be regarded as a laboratory vacuum UV spectrometer of low resolution for studies

* Contribution No. 274 from the Solid State and Structural Chemistry Unit, dedicated to Dr. Raja Ramanna on his 60th birthday.

† To whom all correspondence should be addressed.

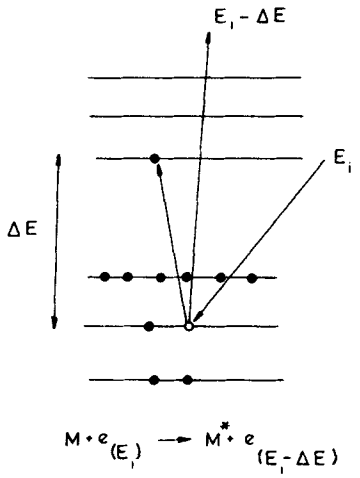

Figure 1. Schematic illustration of the electron energy loss technique for electronic excitations.

involving identification and characterization of molecules in the vapour phase. EELS has the disadvantage of low resolution, a feature common to all techniques of electron spectroscopy. In this paper we report the design and fabrication of a simple EEL spectrometer devoted to the study of atoms and molecules in the gas or vapour phase. We discuss the EEL spectra of several organic molecules recorded with this indigenous spectrometer, having calibrated the spectrometer with gases such as He, O_2 and N_2.

2. Design of the spectrometer

The spectrometer consists of an electron beam source, a monochromator, electron lenses, sample chamber, analyser and a detector. As most of the electronic excitations in the UV and vacuum UV regions lie in the energy range of 4–10 eV, the energy of a typical source should be about three to five times this energy. We have therefore selected a source energy in the range of 30–70 eV. The design criteria for fabrication of the spectrometer were based on the three important factors discussed below.

2.1 *Incident electron beam intensity*

As the electron beam passes through each of the components of the spectrometer, there is a certain loss in intensity. This loss is minimized by the use of appropriate electron optics; the number of inelastically scattered electrons would also be small, being typically two orders of magnitude less than the incident beam. In view of these factors, it is necessary to have an intense elastic peak of at least 10^5 counts/sec at the mouth of the detector. This would correspond to a current of 10^{-14} amps. Assuming a loss in intensity of the order of 10^4 in the monochromator, 10^3 in the sample chamber and a further loss of 10 in the analyser, the total loss over all the components would be of the order of 10^8. The electron gun source must therefore be capable of emitting in the range of 1–10 microamps in the energy range 30–70 eV. The electron source was designed with these specifications in view.

2.2 *Resolution*

The desired resolution of a spectrometer of this kind meant for the study of organic molecules (operating under low resolution), is approximately 400 meV for a primary energy of about 50 eV. Resolution of this order can be obtained using spherical sector analysers (Kuyatt and Simpson 1967). The resolution $\Delta E/E$ of spherical sector analysers is given by the formula $\Delta E/E = S/2R_0$ where S is the slit width and R_0 is the mean radius of the analyser. If we use a convenient slit width of 1 mm, an analyser of a mean diameter of 125 mm is needed.

2.3 *Vacuum conditions*

Since the spectrometer is devoted to the study of atoms or molecules in the gas or the vapour phase, it is clear that two separate and independent pumping systems are required. One provides the base vacuum required for monochromator and the spectrometer chambers, while the other provides differential pumping for the stream of sample molecules. The sample pressure required to record an EEL spectrum depends on the nature of the sample, as well as the length of the sample chamber. The sample pressure must be such that the mean free path of the electrons for electron impact excitation must be less than the length of the collision chamber. The mean free path λ is defined as $\lambda = 1/n\sigma$, where n is the number of molecules per c.c. and σ is the inelastic electron impact collision cross-section. Assuming σ to be in the range 10^{-15}–10^{-16} cm^2 (McDaniel 1964) for a λ of approximately 25 mm, the sample pressure required is of the order of 10^{-4}–10^{-3} torr. The desired base vacuum of the spectrometer on the other hand is of the order of 10^{-6} torr. Hence the crucial need would be for an effective differential pumping of the sample. The vacuum system was designed keeping these requirements in view.

3. Fabrication of the spectrometer

3.1 *Electron source*

A schematic diagram of the electron gun used in the spectrometer is shown in figure 2. A thoriated tungsten filamet of 0·1 mm dia is mounted on a pair of Ni rods. The filament is

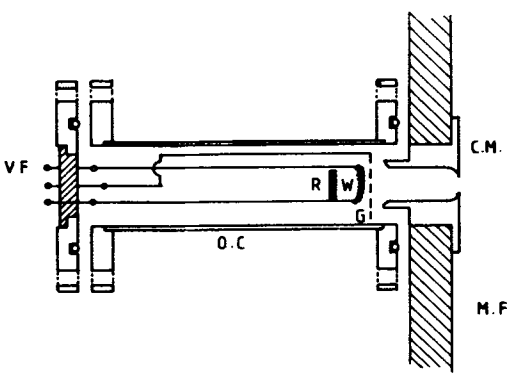

Figure 2. Schematic diagram of the electron gun used in the spectrometer. OC: outercasing; VF: vacuum feed through; R: reflecting electrode; W: tungstun filament; G: grid; CM: collimator; MF: main flange.

resistively heated with a constant current-stabilised power supply fabricated in the laboratory. The electron beam current is controlled by using a negatively biased grid. The gun is mounted on a 63 mm diameter brass flange and enclosed in a stainless steel casing as shown in figure 2. Electrons with energy of 30–70 eV were obtained in this manner.

When the filament is fitted to a reflecting electrode R, which is at the same voltage as the filament, an emission current of 5–10 μamp can be obtained.

3.2 *Monochromator and analyser*

The monochromator as well as the analyser consist of two hemispherical sectors of mean diameter 125 mm. The hemispherical sectors have been machined out of Al blocks to an accuracy of $\pm$0·025 mm. The hemispherical sectors are gold-coated by vacuum deposition employing planetary rotation, to ensure uniform coating of the spherical surfaces. The sectors are then mounted on a 6 mm thick aluminium support plate with suitable electrical insulation (figure 3); the electrical insulations are also shown in the figure.

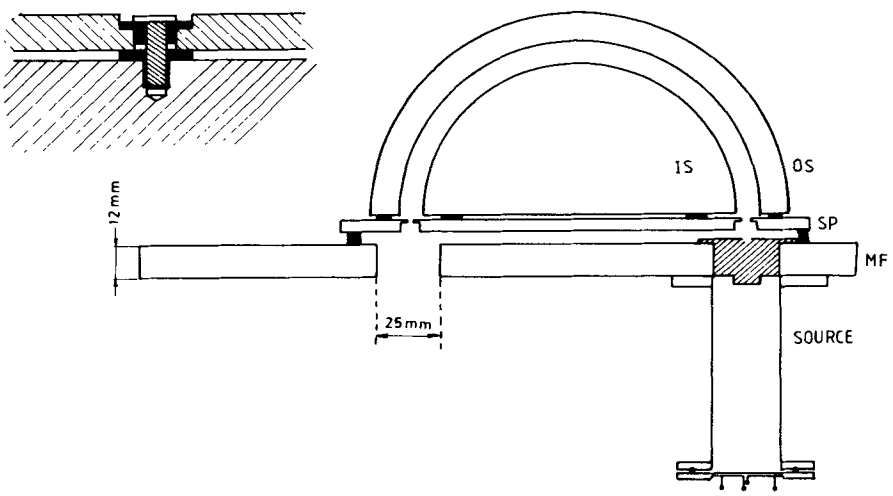

Figure 3. Schematic illustration of the analyser assembly. Shaded areas are machined out of teflon. IS: inner sphere; OS: outer sphere; SP: support plate; MF: main flange. Inset shows the details of insulation employed in the assembly of the analyser.

The performance of the spherical sector analysers was measured over a wide range of electron beam energies (25–100 eV) of interest to us. The analyser response was found to be linear over the 30–70 eV range. Analysers of mean diameter 114 mm and 139 mm, have also been machined and tested for their linear response. The analyser performance was found to improve on coating the slits with gold.

3.3 *Electrostatic lenses*

An electrostatic lens systems was machined as described elsewhere (Spangenberg and Field 1943; Lassettre *et al* 1963). The lens assembly (figure 4) consists of a pair of

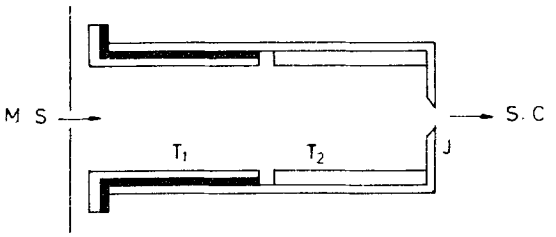

Figure 4. Schematic illustration of the electrostatic lens assembly employed in the spectrometer. T_1 and T_2 are cylindrical tubes comprising the lens system. The shaded area is machined out of teflon. MS: monochromatiser slit; J: outer jacket; SC: sample chamber slit.

identical hollow cylindrical tubes mounted co-axially in an outer jacket and insulated electrically from one another, the tubes being separated from each other by a distance equal to one-tenth of their diameter. The lens system mounted on the "out" slit of the monochromator, acts as a collimator and helps to focus the beam emerging from the monochromator into the sample chamber. The cylindrical lenses were machined from stainless steel rods of suitable dimensions to an accuracy of $\pm 0{\cdot}025$ mm and coated with gold. The lens system was found to work with negligible chromatic aberration.

3.4 *Sample chamber*

The sample chamber was constructed out of a stainless steel bellow 25 mm in diameter and 25 mm in length. It was fitted between two brass collars, which were in turn welded to the sample input and output lines. The gaseous sample is introduced through a sensitive needle valve. When the sample pressure in the sample chamber was 10^{-3}–10^{-4} torr, the base vacuum in the spectrometer chambers increases from 2×10^{-6} torr to 4×10^{-6} torr. The electron beam emerging from the lens system meets the stream of sample molecules at right angles in the sample chamber.

The flexibility of the bellow permits us to collect the scattered electron current along off normal angles. A study of the angular dependence of the scattered electron current can provide information on the shapes and symmetries of orbitals.

3.5 *Detector and ratemeter*

A Mullard channel electron multiplier (B419BL) was used to amplify the electrons coming from the energy analyser; this is the only imported component in the spectrometer. The electron multiplier responds to an input of one electron upto about 10^8 electrons and its duration (full-width at half-maximum) is about 10 nanosecond. The maximum operating voltage of the multiplier is around 3·5 kV, the nominal gain at 2·5 kV being about $1{\cdot}1 \times 10^8$ at a nominal resistance of 5×10^9 ohm.

The high impedence transducer (detector) such as the electron multiplier requires an amplifier which converts a transfer of charge into a change of voltage. In the ratemeter (figure 5), we used a hybrid charge-sensitive preamplifier-discriminator (AMPTEK A-101 PAD) to convert pulses of charge to pulses of voltage. This is capable of handling counts upto a maximum of 4×10^6 with pulse pair resolution of 250 nsec. The input threshold could be varied from $1{\cdot}6 \times 10^{-13}$ coulomb to 15×10^{-12} coulomb.

The output from the charge-sensitive amplifier is fed to the decad counter and monostable multivibrator. This positive pulse is fed to the voltage level translator

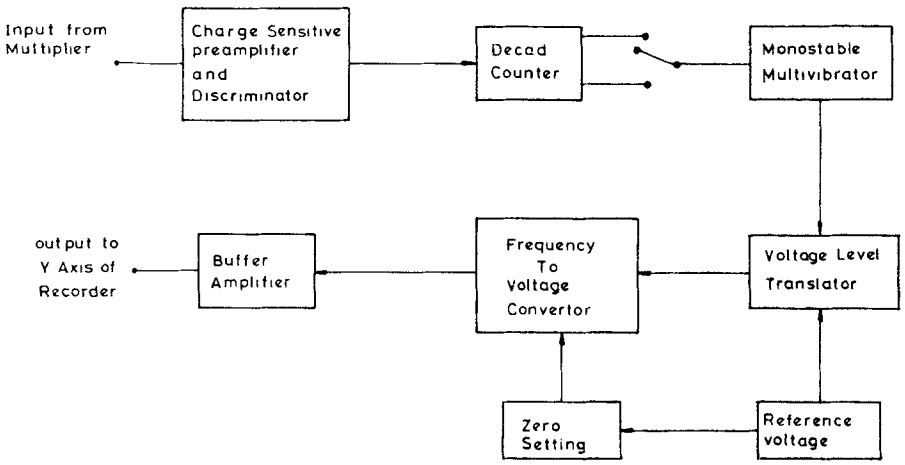

Figure 5. Block diagram for the construction of ratemeter.

which produces the constant 12 V positive pulse. This constant height pulse is fed to the 'frequency to voltage' converter and buffer. Reference voltage is used to bias the voltage level translator and also to introduce zero bias to 'frequency-to-voltage' converter. The output DC voltage from the ratemeter is fed to the *Y* axis of the X-Y recorder which directly gives the number of counts per second.

3.6 *General assembly and the vacuum system*

The spectrometer consists of two main chambers 241 mm in diameter and 228 mm in length fitted to brass collars of 304 mm diameter. The main chambers are made by rolling 3 mm stainless steel plates into cylinders with all the joints being accomplished by silver brazing. Both the chambers have been provided by two more sheets of μ-metal for shielding the earth's magnetic field.

The general assembly of the spectrometer is shown in figure 6 and the electronic control in figure 7. The source, monochromator and the electrostatic lens are fitted to a 300 mm diameter Al flange 12 mm in thickness, and is fitted to the first chamber. The monochromator chamber is mounted on a 150 mm diameter oil diffusion pump which is backed by a 300 lit/min rotary pump. This consists of the main pumping system and is capable of providing an ultimate vacuum of better than 2×10^{-6} torr, with a total pump down time of less than 30 min.

The analyser and detector are mounted on a 300 mm diameter Al flange of 12 mm thickness. This flange is fitted to the analyser vacuum chamber. The analyser chamber is also connected to the main vacuum system through a 25 mm diameter flexible tubing. The collision chamber is fitted between the two spectrometer chambers linking the monochromator output to the analyser input. The collision chamber is fitted to a 100 mm oil diffusion pump backed by a 300 lit/min rotary pump for differentially pumping the sample.

Both the spectrometer chambers are provided with pirani and hot cathode ionisation gauges for measurement of vacuum. The sample pumping line is also fitted with separate gauge heads for measuring the sample pressure. A photograph of the instrument in final assembly is shown in figure 8.

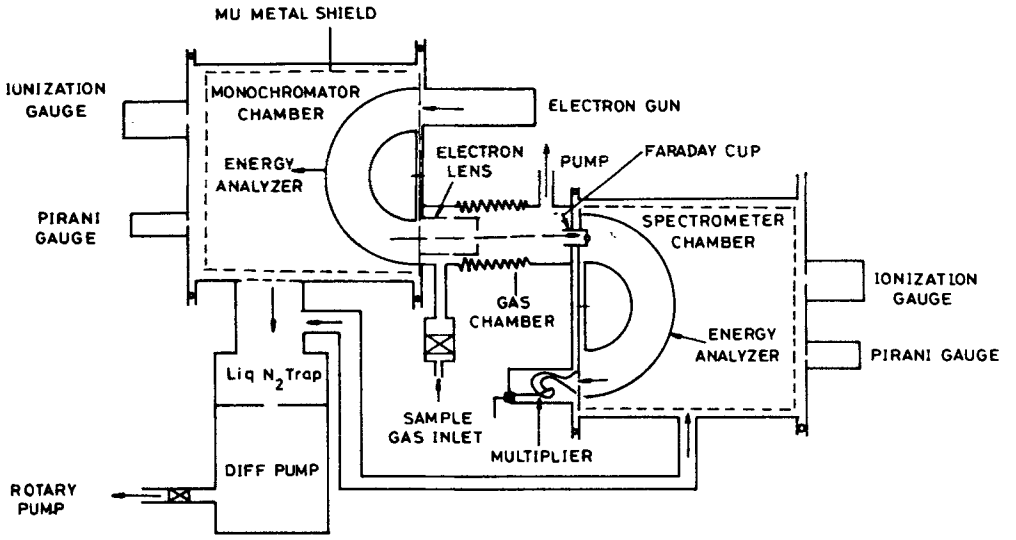

Figure 6. General assembly of the spectrometer.

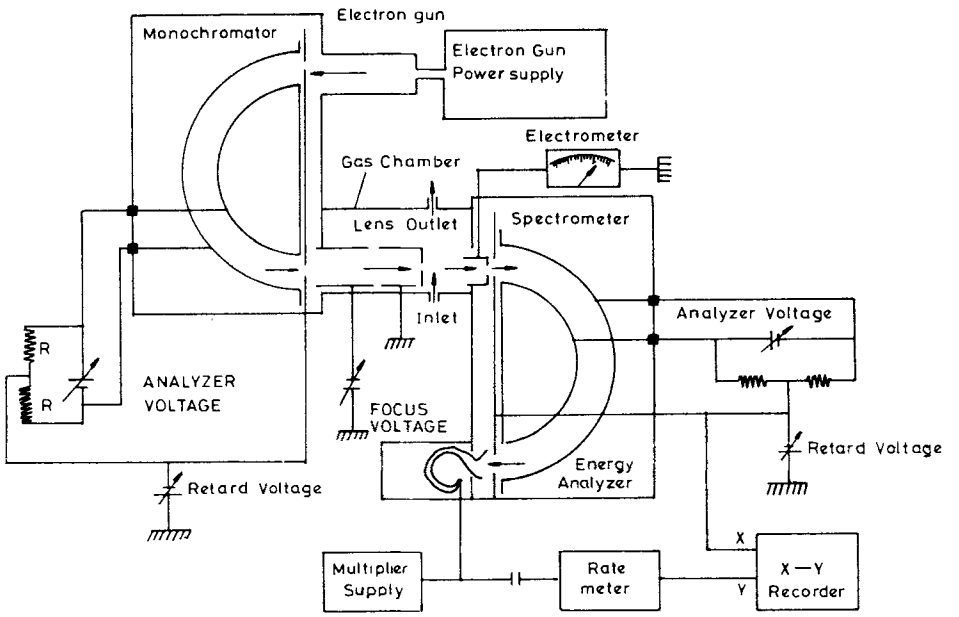

Figure 7. Schematic illustration of the electronic controls employed in the spectrometer.

4. Operation of the spectrometer

The vacuum system is first switched on. On achieving the base vacuum of the system (2×10^{-6} torr), the source gun is put on and degassed for 10 to 15 min. The

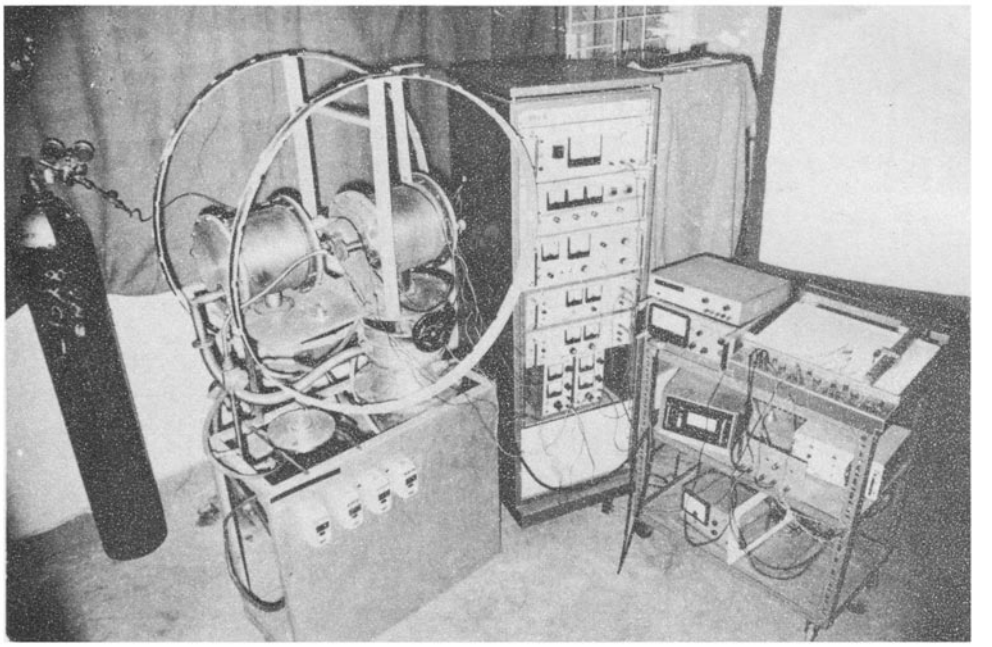

Figure 8. Photograph of the working spectrometer in final assembly.

collision chamber is pumped through the sample pumping line till the base vacuum in the sample pumping line (4×10^{-6} torr) is of the same order as that in the main pumping system. The source energy is selected to be in the 50–70 eV range and the monochromator and lens voltages are suitably altered until the Faraday collector C (see figure 6) mounted at the mouth of the analyser collects a maximum beam current ($\sim 10^{-12}$–10^{-9} amps). This beam enters the analyser. A high voltage of 2·2–2·5 kV is applied to the multiplier and the ratemeter is switched on. The analyser voltage is scanned using a DC ramp. The spectra are recorded by scanning the voltage across the analyser by keeping the retard voltage at zero. We can also scan the retard voltage applied to the analyser mounting plate by applying a constant DC voltage to the hemispheres. The elastic peak is first recorded at low sensitivity of the ratemeter and having found the elastic peak, the sample is introduced into the collision chamber, until the sample pressure rises to 10^{-4}–10^{-3} torr. The elastic peak height drops to half its original value at this juncture and in order to detect the loss peaks, the ratemeter is then fixed to high sensitivity (typically 300 to 10^3 times higher than the sensitivity used to record the elastic peak).

5. Performance of the spectrometer

The spectrometer is readily calibrated by recording the spectra of standard gases such as He, N_2, O_2 and benzene vapour. The spectrum of He is shown in figure 9a, where peaks due to excitations into the various excited states are clearly assigned. The peak due to the $1^1S \rightarrow 2^1S$ excitation can also be assigned, thus demonstrating the versatility

of the spectrometer in detecting optically forbidden transitions. The optically allowed transitions to the 2^1P, 3^1P and 4^1P excited states are seen as prominent peaks and are eminently suited for calibration. In figure 9b, we show the spectra of pure N_2, pure O_2 and air. The spectrum of air appears as due to a mixture of N_2 and O_2. The electronic excitations responsible for these peaks are described in the literature (Lassettre *et al* 1963; Kuppermann *et al* 1968).

At a primary beam energy of 50 eV, the fwhm of the elastic peak is 360 meV. The resolution of the spectrometer is 0·72 % at 50 eV and the uncertainty in measurement is ± 0·05 eV.

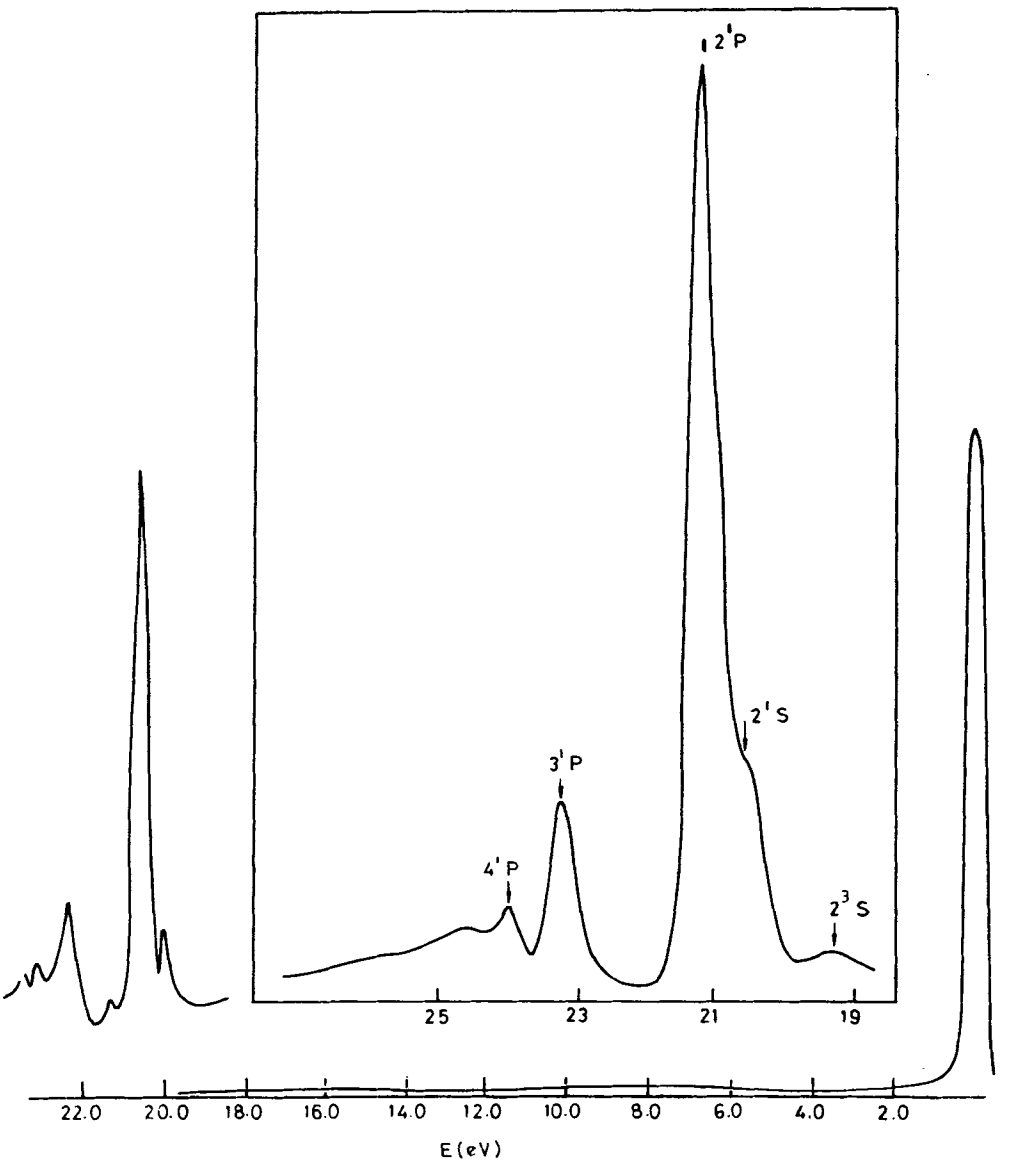

Figure 9. (a) EEL spectrum of He gas recorded in the spectrometer. Inset shows the spectrum on a expanded scale, together with the assignment of the transitions.

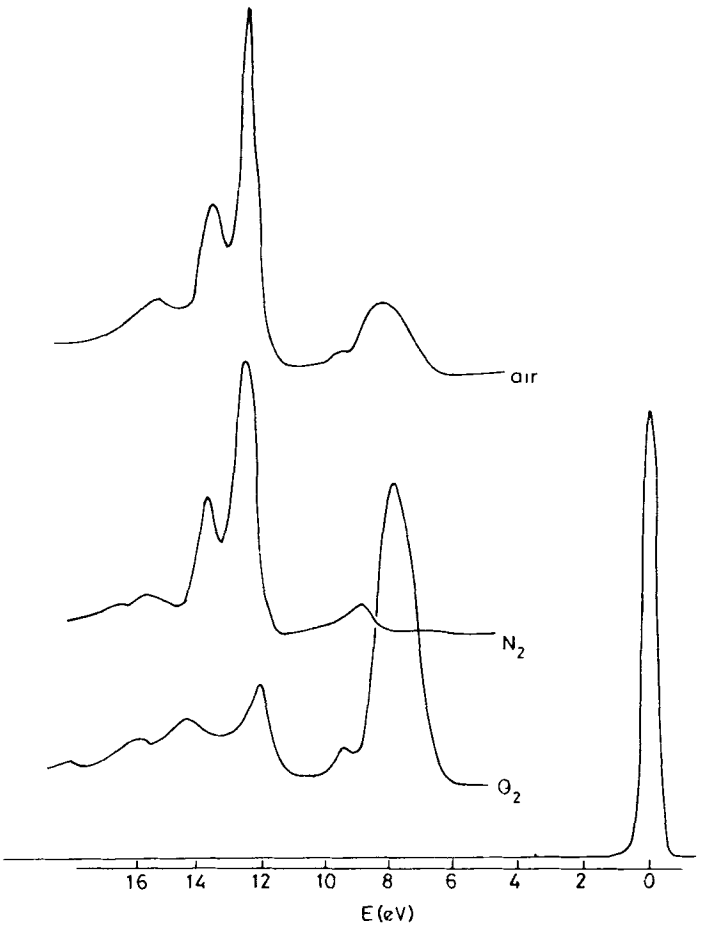

Figure 9. (b) EEL spectrum of N_2, O_2 and air recorded for the purpose of calibration.

6. Study of EEL spectra of organic molecules

6.1 *Aliphatic alcohols and diethylether*

In figure 10 we show the EEL spectra of a few aliphatic alcohols and diethylether. The absorption maxima observed in these compounds are listed in table 1. These molecules can show transitions due to the $n \rightarrow \sigma^*$ and $\sigma \rightarrow \sigma^*$ excitations (Rao 1975). The $n \rightarrow \sigma^*$ transition would be associated with lower energies and intensities compared to the $\sigma \rightarrow \sigma^*$ transitions which occur in the vacuum UV region with high extinction coefficients. Accordingly in EEL spectra, the first band occurs at 177 nm (7 eV) in CH_3OH which compares well with the UV absorption band of 174 nm reported by Tsubomura *et al* (1964). This band is due to the $n \rightarrow \sigma^*$ transition involving the oxygen lone pair. The first band in CH_3OH is quite intense and sharp, but as the alkyl group becomes bulkier, the first band becomes broader and less intense. The broadening of

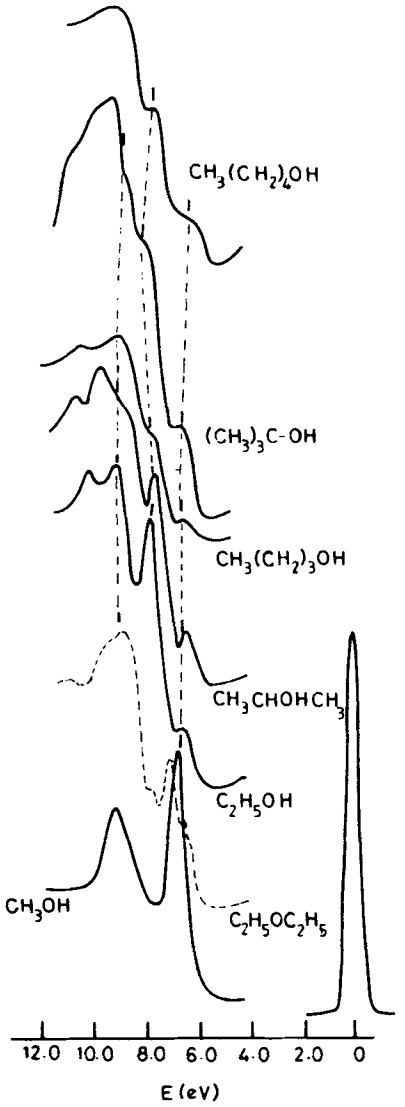

Figure 10. EEL spectra of aliphatic alcohols.

the $n \rightarrow \sigma^*$ band is expected as bulkier alkyl groups provide a wide spectrum of excited σ^* states. Secondary and tertiary alcohols exhibit the $n \rightarrow \sigma^*$ band at lower energies compared to the primary alcohols due to enhanced inductive effect of the alkyl groups in the former.

In addition to the $n \rightarrow \sigma^*$ band, we see additional bands at higher energies in EEL spectra of all the alcohols. These bands are broad and increase in complexity as the alkyl groups become bulky. These bands may be divided into two categories. The first category appears in the 158–151 nm (7·8–8·2 eV) range and is absent in CH_3OH. It appears as a distinct peak in C_2H_5OH and i-C_3H_7OH, but becomes a shoulder in the

Table 1. Absorption maxima in the vacuum UV region for some aliphatic alcohols and halocarbons[a].

Compound	$n \rightarrow \sigma^*$		$\sigma \rightarrow \sigma^*$[b]	
CH_3OH	177(6·98)		141(8·78)	130(9·5)
EtOH	190(6·49)	156(7·94)	132(9·39)	115(10·7)
$C_2H_5OC_2H_5$	187(6·62):173(7·16)		139(8·9)	125(9·87)
isopr-OH	191(6·5)	161(7·7)	139(8·9)	127(9·75) 114(10·82)
npr-OH	177(6·98)	156(7·94)	141(8·78)	125(9·86)
t-Bu-OH	184(6·74)	151(8·18)	133(9·26)	117(10·59)
n-BuOH	198(6·26)	158(7·82)	133(9·26)	
CH_2Cl_2	171(7·22)	151(8·18)	139(8·90)	
$CHCl_3$	177(6·98)	145(8·54)	133(9·26)	
CCl_4	174(7·09)	141(8·78)	133(9·26)	

[a] Values in parentheses are transition energies in eV.
[b] At low wavelengths, some Rydberg transitions may be mixed with the $\sigma \rightarrow \sigma^*$ transitions.

higher members of this series. This feature is likely to be due to the $\sigma \rightarrow \sigma^*$ transition; since it is absent in CH_3OH, we may assign it to the $\sigma \rightarrow \sigma^*$ transition involving the C–C bond.

The second category of $\sigma \rightarrow \sigma^*$ transitions occurs at wavelengths below 150 nm (> 8·2 eV). There is a band appearing in the 140–130 nm (8·8–9·5 eV) range and another at or below 130 nm; the first is probably due to the $\sigma \rightarrow \sigma^*$ transition involving the C–H bond. Below 130 nm (> 9·5 eV) excitation into the Rydberg states probably occurs.

In diethylether, the $n \rightarrow \sigma^*$ band of ethanol splits into two bands, one at lower and the other at higher energy relative to ethanol.

6.2 *Carbonyl compounds*

In figure 11 we show the EEL spectra of a few carbonyl compounds. The carbonyl group exhibits $n \rightarrow \pi^*$, $n \rightarrow \sigma^*$ and $\pi \rightarrow \pi^*$ transitions in the electronic spectra (Rao 1975); the $n \rightarrow \pi^*$ transition has a low extinction coefficient and is not seen in the EEL spectra recorded by us. The first band seen in EEL spectra appears in the energy range 180–190 nm (6·5–6·8 eV) in acetaldehyde and acetone and this can be readily assigned to the $n \rightarrow \sigma^*$ transition of the carbonyl group. In acetone, it appears as a sharp peak, while in acetaldehyde it is a shoulder on a higher energy peak. In methylacetate also it appears as a weak shoulder. This band is however not seen in formaldehyde, which shows a single sharp peak at 172 nm (7·2 eV) due to the $\pi \rightarrow \pi^*$ transition. The $\pi \rightarrow \pi^*$ transition occurs with high intensity in the 166–172 nm (7·2–7·5 eV) range in all the carbonyl compounds studied by us (see table 2). Below 155 nm (8·0 eV), carbonyl compounds show a broad band with a multiplicity of peaks due to the $\sigma \rightarrow \sigma^*$ transitions.

In formic and acetic acids, the peak due to the $\pi \rightarrow \pi^*$ transition occurs at 153 nm (Rao 1975), while in acetic anhydride it is around 166 nm (7·5 eV) just as in other carbonyl compounds. Formic acid shows no other peak, but both acetic acid and its anhydride exhibit a broad band around 125 nm (9·9 eV) due to the $\sigma \rightarrow \sigma^*$ transitions of the methyl group (figure 12). Presence of several Rydberg states causes broadening

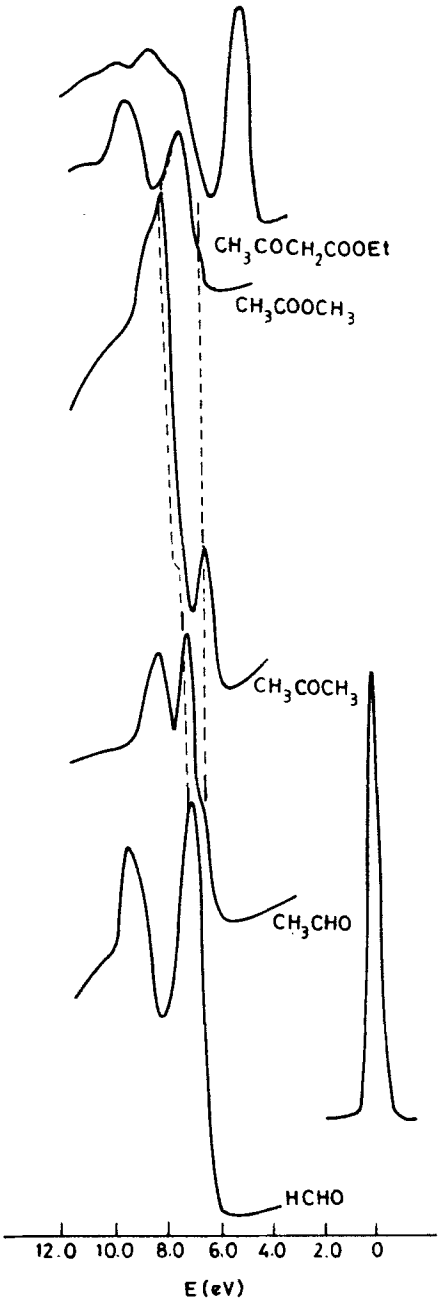

Figure 11. EEL spectra of aliphatic carbonyl compounds.

of the $\sigma \rightarrow \sigma^*$ band in the higher energy region. Both the acids show a slight broadening of the $\pi \rightarrow \pi^*$ peaks possibly due to dimerization.

EEL spectra of a series of aliphatic amides are shown in figure 13. The band due to the $\pi \rightarrow \pi^*$ transition shifts considerably from 168 nm (7·4 eV) in formamide to 202 nm

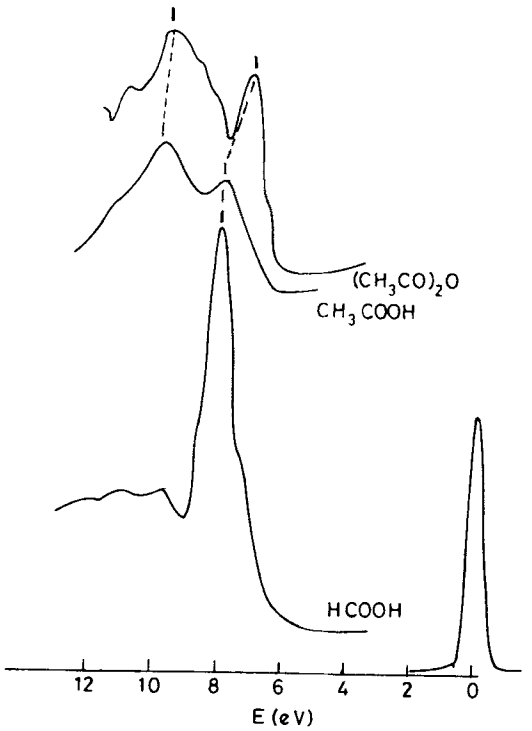

Figure 12. EEL spectra of formic and acetic acids together with the spectrum of acetic anhydride.

Table 2. Absorption maxima seen in the vacuum UV region for a series of carbonyl compounds[a].

Compound	$n \rightarrow \sigma^*$	$\pi \rightarrow \pi^*$	$\sigma \rightarrow \sigma^*$[b]	
HCHO	—	172(7·22)		
CH_3CHO	180(6·85)	169(7·34)	147(8·42)	
CH_3COCH_3	192(6·44)	—	152(8·12)	
CH_3COOCH_3	180(6·85)	166(7·46)		130(9·51)
$(CH_3CO)_2O$	—	166(7·46)	—	128(9·62)
CH_3COOH	—	153(8·1)	—	124(9·98)
HCOOH	—	166(7·45); 153(8·1)	—	
$HCONH_2$	—	168(7·34)	—	
HCONH(Me)	—	177(6·98)	—	
$HCON(Me)_2$	—	202(6·13)	—	
$CH_3CON(Me)_2$	—	194(6·37)	—	

[a] Values in parentheses are transition energies in eV.

[b] Rydberg transitions may be mixed up with the $\sigma \rightarrow \sigma^*$ transitions at low wavelengths.

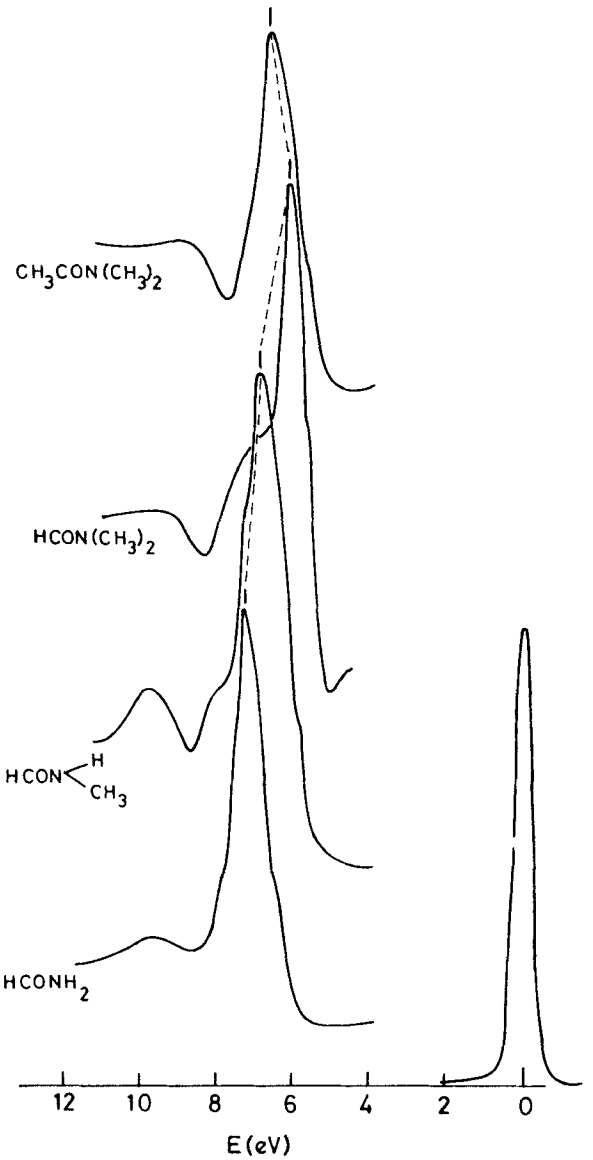

Figure 13. EEL spectra of aliphatic amides.

(6·1 eV) in N-N dimethylformamide. Similar shifts are seen in the acetamide series as well (table 2).

6.3 *Benzene derivatives*

In figures 14 and 15, we show the EEL spectra of benzene and several of its mono- and di-substituted derivatives. Benzene exhibits three bands in the electronic absorption spectra, two of these in the ultraviolet region (203 and 260 nm) and one in the far

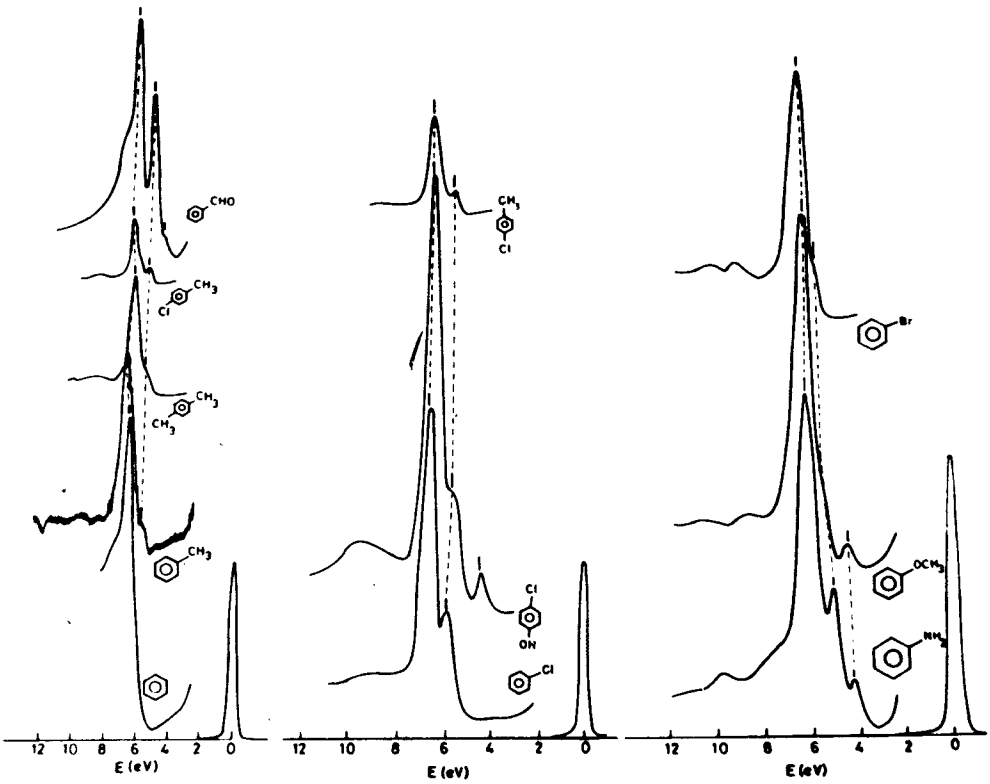

Figure 14. EEL spectra of a few benzene derivatives.

Table 3. Absorption maxima in vacuum UV region for some aromatic molecules[a].

	β(nm)	p(nm)	α(nm)
C_6H_6	184(6·74)		
Toluene	181(6·86)		
p-xylene	190(6·49)		
Chlorobenzene	190(6·49)		
Bromobenzene	184(6·74)		
Anisole	189(6·55)	214(5·77)	271(4·57)
Benzaldehyde	198(6·25)	234(5·29)	271(4·57)
Aniline	190(6·49)	224(5·53)	278(4·45)
N-Methyl Aniline	196(6·32)	231(5·35)	286(4·33)
N-N-Dimethylaniline	202(6·13)	245(5·05)	278(4·45)
N-N-Diethylaniline	198(6·25)	257(4·81)	294(4·21)
p-Chlorotoluene	190(6·49)	224(5·53)	
p-Chlorophenol	190(6·49)	221(5·59)	282(4·39)

[a] β, p and α bands correspond to the 183, 203 and 260 nm bands of benzene respectively. Values in parantheses are transition energies in eV.

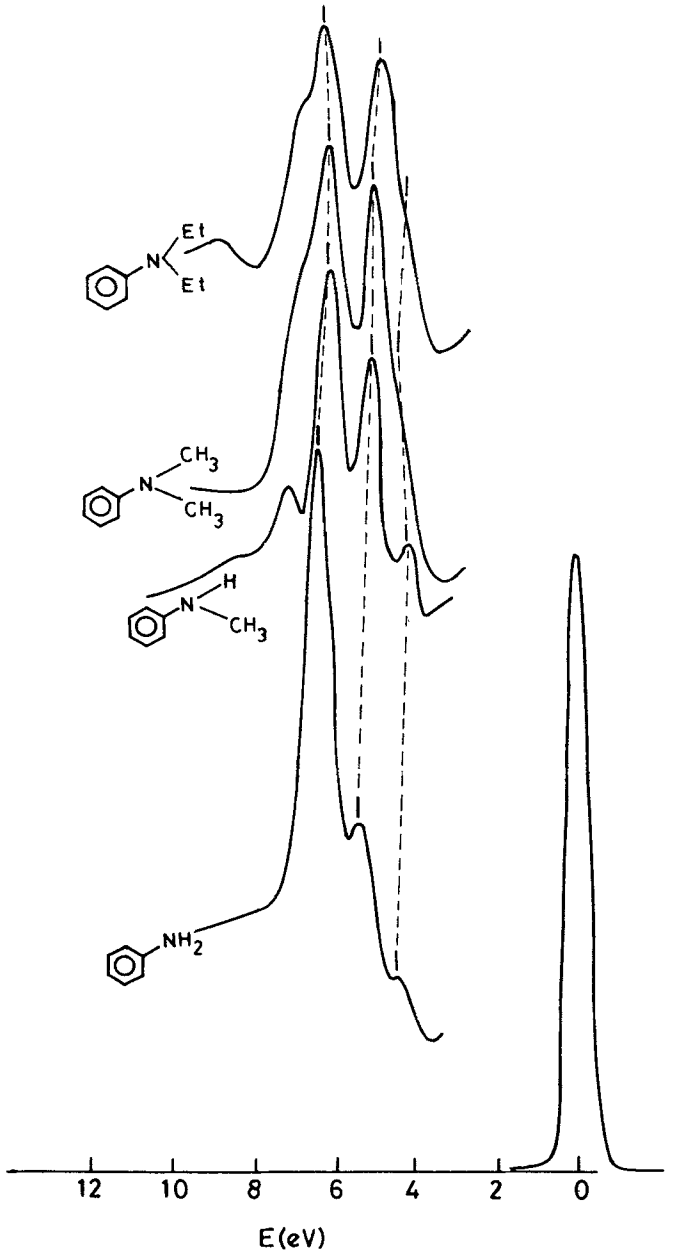

Figure 15. EEL spectra of a few benzene derivatives.

ultraviolet region (180 nm). The last of these is the most intense with an extinction coefficient of 10^5 (Rao 1975). The high symmetry of the benzene molecule causes the lower energy bands to have low intensities. Consequently in EEL spectra recorded by us, we only see the 180 nm (6·9 eV) band as a sharp feature. In the mono- and di-substituted derivatives, the D_{6h} symmetry of the benzene molecule is destroyed and we begin to see

the lower energy bands as well. This is exemplified in benzaldehyde, where the 234 nm (5·3 eV) band has comparable intensity with the 180 nm band. Substituents cause a red shift of the 180 nm band of benzene (table 3). The shift is specially significant in aniline and its methylated derivatives, where the amino group can donate electrons to the aromatic ring.

Acknowledgement

The authors are thankful to the Department of Science and Technology, Government of India and University Grants Commission, for support of the instrument fabrication and research reported in this paper.

References

Celotta R J and Huebner R H 1979 in *Electron spectroscopy, theory, techniques and applications* (eds) C R Brundle and A D Baker (New York: Academic Press) pp. 41

Koerting C F, Walzl N K and Kuppermann A 1984 *Chem. Phys. Lett.* **109** 140

Kuppermann A, Flicker W M and Mosher O A 1979 *Chem. Rev.* **79** 77

Kuppermann A, Rice J K and Trajmar S 1968 *J. Phys. Chem.* **72** 3894

Kuyatt C E and Simpson J A 1967 *Rev. Sci. Instrum.* **38** 103

Lassettre E N, Skerbele A, Dillon M A and Ross K J 1963 *J. Chem. Phys.* **48** 5066

McDaniel E W 1964 *Collision phenomena in ionised gases* (New York: John Wiley)

Oppenheimer J R 1928 *Phys. Rev.* **32** 361

Rao C N R 1975 *Ultraviolet and visible spectroscopy—Chemical applications*, 3rd edn (London: Butterworths)

Rao C N R, Srinivasan A, Jagannathan K and Hegde M S 1980 *J. Sci. Ind. Res.* **39** 212

Spangenberg K R and Field L M 1943 *Elec. Commun.* **21** 14

Tsubomura H, Kimura K, Kaya K, Tanaka J and Nagakura S 1964 *Bull. Chem. Soc. Jpn* **37** 417